1-1-2012

Airborne electromagnetic imaging of discontinuous permafrost

Burke J. Minsley
U.S. Geological Survey, Denver, Colorado

Jared D. Abraham
U.S. Geological Survey, Denver, Colorado

Bruce D. Smith
U.S. Geological Survey, Denver, Colorado

James C. Cannia
U.S. Geological Survey, Lincoln, Nebraska

Clifford I. Voss
U.S. Geological Survey, Menlo Park, California

See next page for additional authors

Airborne electromagnetic imaging of discontinuous permafrost

Burke J. Minsley,[1] Jared D. Abraham,[1] Bruce D. Smith,[1] James C. Cannia,[2] Clifford I. Voss,[3] M. Torre Jorgenson,[4] Michelle A. Walvoord,[5] Bruce K. Wylie,[6] Lesleigh Anderson,[7] Lyndsay B. Ball,[1] Maryla Deszcz-Pan,[1] Tristan P. Wellman,[8] and Thomas A. Ager[7]

Received 21 October 2011; revised 16 December 2011; accepted 21 December 2011; published 20 January 2012.

[1] The evolution of permafrost in cold regions is inextricably connected to hydrogeologic processes, climate, and ecosystems. Permafrost thawing has been linked to changes in wetland and lake areas, alteration of the groundwater contribution to streamflow, carbon release, and increased fire frequency. But detailed knowledge about the dynamic state of permafrost in relation to surface and groundwater systems remains an enigma. Here, we present the results of a pioneering ~1,800 line-kilometer airborne electromagnetic survey that shows sediments deposited over the past ~4 million years and the configuration of permafrost to depths of ~100 meters in the Yukon Flats area near Fort Yukon, Alaska. The Yukon Flats is near the boundary between continuous permafrost to the north and discontinuous permafrost to the south, making it an important location for examining permafrost dynamics. Our results not only provide a detailed snapshot of the present-day configuration of permafrost, but they also expose previously unseen details about potential surface – groundwater connections and the thermal legacy of surface water features that has been recorded in the permafrost over the past ~1,000 years. This work will be a critical baseline for future permafrost studies aimed at exploring the connections between hydrogeologic, climatic, and ecological processes, and has significant implications for the stewardship of Arctic environments. **Citation:** Minsley, B. J., et al. (2012), Airborne electromagnetic imaging of discontinuous permafrost, *Geophys. Res. Lett.*, *39*, L02503, doi:10.1029/2011GL050079.

1. Introduction

[2] Permafrost– described here as ground that is perennially frozen– is present throughout much of the Arctic and in alpine environments, and underlies approximately 24% of the land area in North America [*Zhang et al.*, 2008]. The distribution of permafrost in Earth's cryosphere impacts hydrogeologic processes [*Walvoord and Striegl*, 2007; *Yoshikawa and Hinzman*, 2003], climate feedbacks [*Froese et al.*, 2008; *Schuur et al.*, 2009], and Arctic ecology [*Avis et al.*, 2011; *Jorgenson et al.*, 2001]. Increased thawing due to warmer temperatures can enhance surface – groundwater interaction through taliks (unfrozen zones within permafrost regions) and alter the contribution of groundwater to streamflow [*Bense et al.*, 2009; *Walvoord and Striegl*, 2007]. In addition, many permafrost soils constitute a substantial carbon pool [*Zimov et al.*, 2006] that has the potential to act as a positive climate change feedback by contributing to atmospheric carbon when thawed [*Koven et al.*, 2011; *Schuur et al.*, 2009]. Changes in wetland areas [*Avis et al.*, 2011] and fire frequency or intensity that result from thawed permafrost also have important ecological and climate implications [*Mack et al.*, 2011; *O'Donnell et al.*, 2011].

[3] Knowledge about the configuration of permafrost at depth is crucial to our understanding of these natural phenomena, and provides guidance for management decisions about resources and infrastructure [*Nelson et al.*, 2001, 2002]. Nevertheless, specific details about the arrangement of permafrost at depth are lacking because of the difficulty in probing the subsurface over areas greater than a few square kilometers. Typically, inferences about permafrost distributions are largely based on conceptual models derived from surface observations [*Duguay et al.*, 2005; *Ferrians*, 1965], sparse borehole measurements [*Osterkamp*, 2007; *Romanovsky and Osterkamp*, 2000], and limited geophysical data [*Froese et al.*, 2005; *Yoshikawa and Hinzman*, 2003].

[4] Airborne electromagnetic (AEM) data presented here play a unique role in characterizing permafrost. Their ability to image physical properties at depth cannot be achieved with satellite systems, and their spatial coverage cannot be matched by ground-based measurements or borehole data. Advances in AEM instrumentation and data processing have greatly improved our ability to image the subsurface, and these data are being increasingly utilized for large-scale groundwater studies [*Siemon et al.*, 2009]. We show that remotely sensed AEM data are able to identify the subsurface configuration of permafrost, and also can be used to infer the thermal legacy of surface and groundwater systems in permafrost regions.

2. Study Area and Methods

[5] Recently acquired frequency-domain AEM data (see Text S1 of the auxiliary material) [*Ball et al.*, 2011] provide unprecedented three-dimensional views of lithology, permafrost

[1]Crustal Geophysics and Geochemistry Science Center, U.S. Geological Survey, Denver, Colorado, USA.
[2]Nebraska Water Science Center, U.S. Geological Survey, Lincoln, Nebraska, USA.
[3]National Research Program, U.S. Geological Survey, Menlo Park, California, USA.
[4]Alaska Ecoscience, Fairbanks, Alaska, USA.
[5]National Research Program, U.S. Geological Survey, Denver, Colorado, USA.
[6]Earth Resources Observation and Science Center, U.S. Geological Survey, Sioux Falls, South Dakota, USA.
[7]Geology and Environmental Change Science Center, U.S. Geological Survey, Denver, Colorado, USA.
[8]Colorado Water Science Center, U.S. Geological Survey, Denver, Colorado, USA.

0094-8276/12/2011GL050079

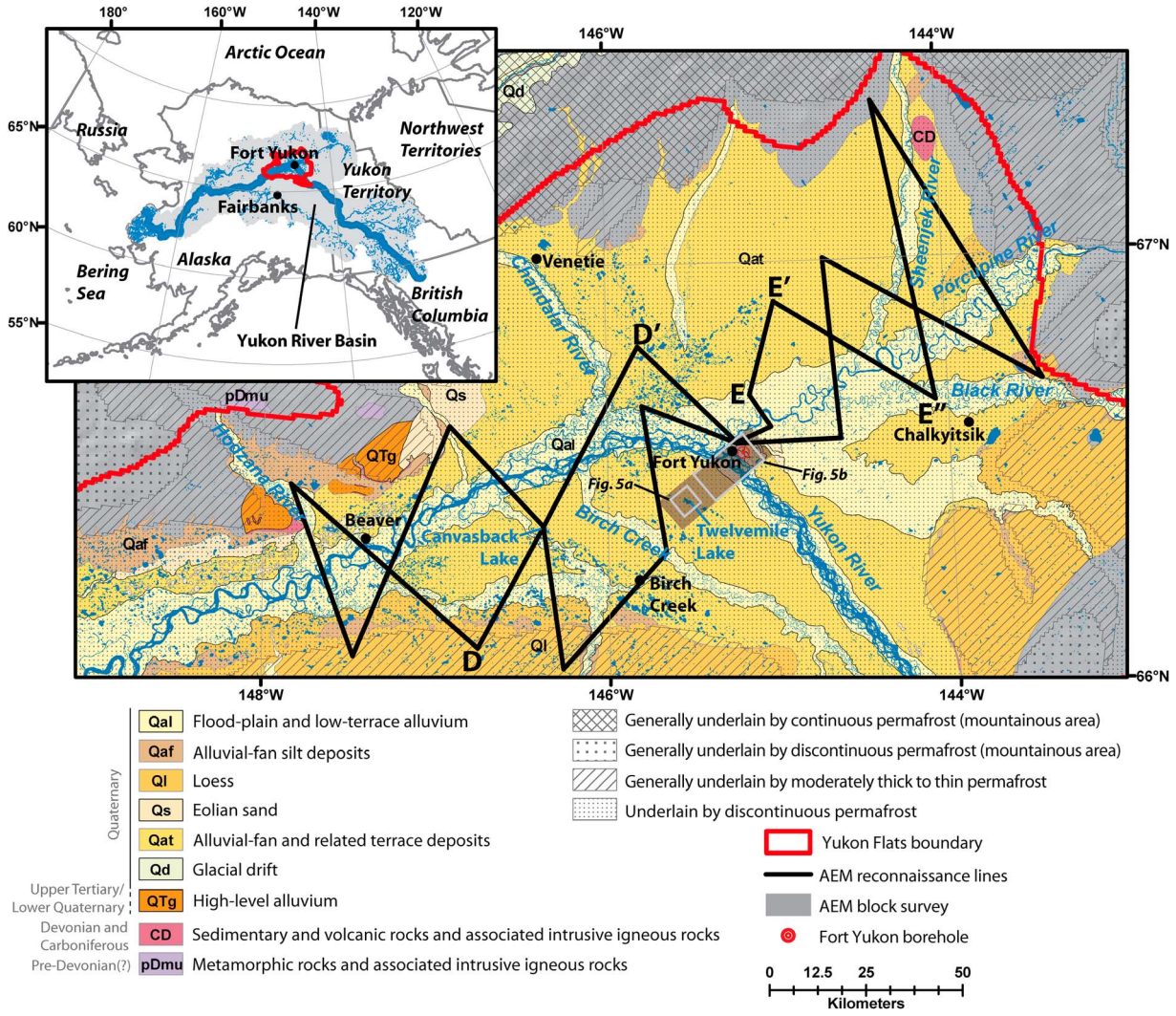

Figure 1. Yukon River Basin location (inset) and geophysical study area with surface water features, surface geology [*Williams*, 1962], and background shading indicating gross permafrost characteristics [*Ferrians*, 1965]. D-D' and E-E′-E″ indicate reconnaissance transects that are discussed in the auxiliary material.

distributions, and potential surface - groundwater connections via taliks beneath lakes and rivers in the Yukon Flats area near Fort Yukon, Alaska (Figure 1).[1] The Yukon Flats (see Text S1 of the auxiliary material for additional background) is a lowland area within the Yukon River Basin, where the Yukon River reaches its northernmost point ~13 km north of the Arctic Circle. The Yukon Flats is of particular importance because it is an area of discontinuous permafrost [*Jorgenson et al.*, 2008] that is generally more unstable and sensitive to a warming climate than continuous permafrost. Because discontinuous permafrost is relatively warm [*Osterkamp and Romanovsky*, 1999], contact with and heat transfer from adjacent unfrozen ground or water bodies can result in significant thawing [*Jorgenson et al.*, 2010; *Osterkamp*, 2007].

[6] AEM data were acquired during one week in June 2010 using the Fugro RESOLVE system, which operates at six frequencies between 0.4 and 129 kHz and is flown at a average speed of 30 m/s and ground clearance of 30 m (see Text S1 of the auxiliary material). The survey consists of a block of closely spaced lines that cover approximately 300 km^2 and a number of widely spaced 'reconnaissance' lines, totaling nearly 900 km in length, that sample a broader range of geologic settings within the Yukon Flats (Figure 1). High-resolution mapping in three dimensions is achieved within the block, and visualization of different hydrogeologic settings and permafrost distributions along the widely spaced lines provides new understanding of the Yukon Flats at both small and large scales. Inversion of ~500,000 AEM soundings [*Ball et al.*, 2011] yields densely sampled models of electrical resistivity along the survey flight lines to depths of ~100 m.

3. Results

[7] We incorporate limited drill hole data near Fort Yukon, including a 1954 water well [*Williams*, 1962] and a nearby borehole that was drilled in 1994 and re-drilled in 2004 [*Clark et al.*, 2009] (Figure 1) to develop a relation

[1]Auxiliary materials are available in the HTML. doi:10.1029/2011GL050079.

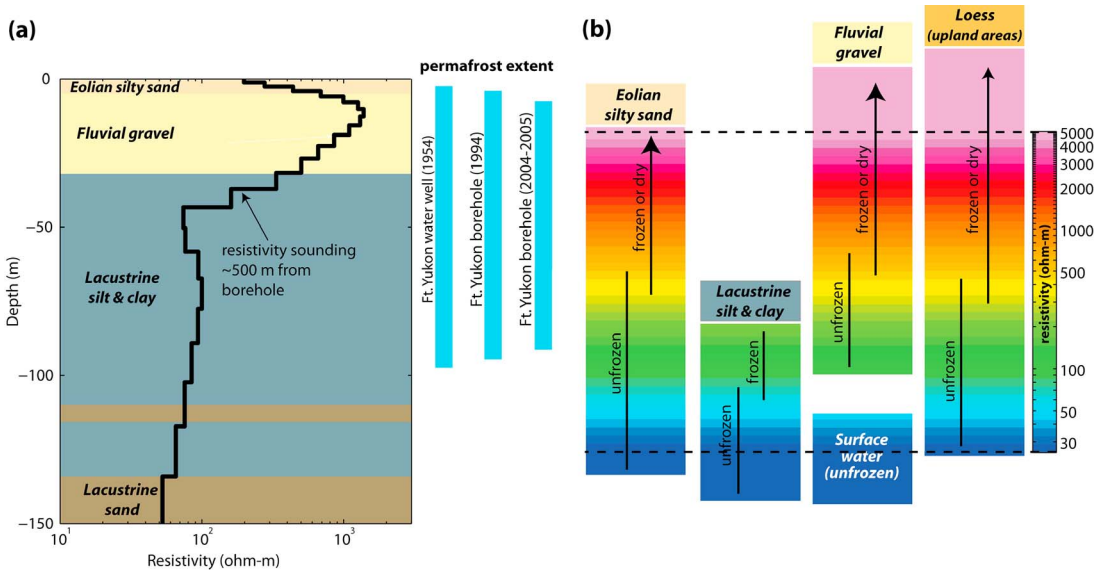

Figure 2. (a) Comparison of an inverted AEM resistivity sounding with nearby borehole lithology and observations of permafrost extent in the borehole and an older water well. (b) Interpretive schematic for the AEM survey, which indicates the typical range of resistivity values for various materials under frozen and thawed conditions [*Hoekstra et al.*, 1975; *Palacky*, 1987].

that connects inverted electrical resistivity values to lithology and permafrost. AEM-derived resistivity values of 100–200 ohm-m are observed in the uppermost unfrozen eolian silt and sand at the borehole location (Figure 2a). Resistivity rapidly increases to greater than 1,000 ohm-m in the upper fluvial gravel unit, which was entirely frozen in 2005 except for the top 2–3 m. A transition to lower resistivity values near or less than 100 ohm-m is observed at depth where frozen lacustrine silt and clay are present. Decreased resistivity in the unfrozen upper 5–10 m and the trend toward lower resistivity values below the depth of permafrost at ~90 m within the lacustrine silt are consistent with the fact that frozen materials have higher resistivity than their unfrozen counterparts [*Hoekstra et al.*, 1975].

[8] Limited well and borehole data, additional knowledge about the depositional environment (see Text S1 of the auxiliary material), and information about typical resistivity values of various earth materials [*Hoekstra et al.*, 1975; *Palacky*, 1987] provide an interpretive framework for the AEM-derived models (Figure 2b). Each material can exhibit a relatively wide range of resistivity values due to variability in porosity, saturation, mixing of different lithofacies, and thermal state. The range of resistivity values for surface waters, which is primarily a function of salinity, is empirically established using AEM data acquired over known water bodies and is also consistent with lake-water conductivity measurements. Typical AEM-derived water resistivity values are on the order of tens of ohm-m, although several locations as low as 2–3 ohm-m were observed. Water conductivity measured in Twelvemile Lake (Figure 1) was 550 μS/cm (18 ohm-m), whereas the AEM-derived resistivity in the upper 4 m of the lake is 10–20 ohm-m. The highest water conductivity measured in the area was 3,995 μS/cm (2.5 ohm-m), which is consistent with the lowest values in the AEM survey. Loess can exhibit a wide range of resistivity values, but is only observed over limited portions of the reconnaissance lines at higher elevations in the southern part of the survey (Figure 1), and is easily identified.

[9] Notable features in the AEM-derived resistivity models that are presented as horizontal depth-slice maps (Figure 3) and vertical cross-sections (Figure 4) include: (1) surface water bodies consistently appear as regions of low-resistivity (blue) in the near-surface, several of which extend throughout the entire depth-extent of the model; (2) very high resistivity values greater than 1,000 ohm-m (orange-pink) are observed throughout the upper 15–30 m in the northeast and up to 45 m in the southwest portions of the survey area, and overlie decreased resistivity (blue-green) regions at depth; and (3) the Yukon River is characterized by a broad, relatively low-resistivity zone that widens to the southwest with depth. The subsurface resistivity images, which are interpreted below, provide reliable information from the near-surface to depths of ~100 m throughout the survey area.

4. Discussion

4.1. Lithologic and Permafrost Inferences

[10] Based on the known depositional history of the Yukon Flats and the available stratigraphic data near Fort Yukon (Figure 2a), it appears that lithology has a significant impact on resistivity. The resistive upper gravel deposit observed in the borehole appears to extend across the entire survey block, thickening to the southwest (Figure 4). A wide range of elevated resistivity values is observed within the gravels, where details in the near-surface have been created to varying extents by more recent fluvial and eolian activity. The brown-dashed lines in Figure 4 indicate our interpreted base of the gravel deposit, which is underlain by areas of intermediate (~ 100 ohm-m) to low (<50 ohm-m) resistivity silts and clays. This geologic model is consistent with ground-based electrical resistivity and ground penetrating radar surveys performed along the Yukon River channel both within and outside the AEM survey area [*Froese et al.*, 2005].

[11] A second factor that appears to influence resistivity is the thermal state of the different subsurface materials. Resistivity values within the upper gravels decrease beneath

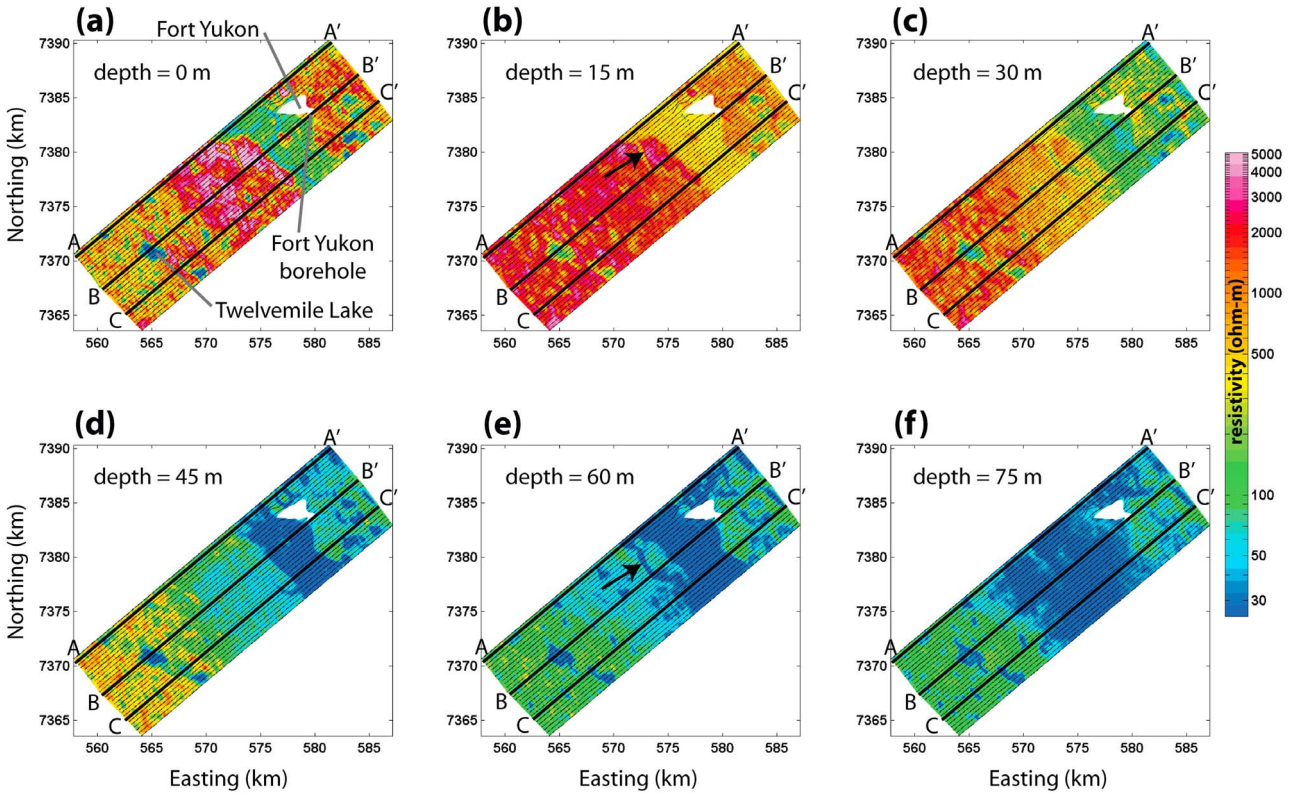

Figure 3. (a–f) Plan-view slices at depth increments of 15 m through the inverted resistivity models within the AEM survey block. Thin black lines indicate the actual flight path during the survey. Transects denoted A-A', B-B', and C-C' indicate the locations of selected cross-sections illustrated in Figure 4. The black arrows in Figures 3b and 3e highlight the location of a sinuous side-channel of the Yukon River that is also shown in Figure 4.

surface water features such as Twelvemile Lake and the Yukon and Porcupine Rivers (Figure 4), which is consistent with these areas being unfrozen or partially frozen (Figure 2). The resistive island in the middle of the Yukon River (Figure 4b) lies between braided river channels and likely has frozen areas as indicated by the presence of old-growth spruce vegetation (*Picea glauca, P. mariana*). This also suggests that it is an older landform because younger bars tend to be dominated by deciduous trees (*Populus tremuloides, Betula neoalaskana*).

[12] Beneath the frozen gravels in the borehole, frozen silts, clays, and sands coincide with intermediate resistivity values of approximately 100 ohm-m from the AEM survey (Figure 2a). Immediately southwest of the Yukon River bank, however, there is a sharp lateral transition to low-resistivity values at depth that dip gradually downward to the southwest away from the river (Figure 4). We interpret this area as an active surface-groundwater 'window' at the location of the present-day Yukon River that is manifested as an unfrozen zone within the lacustrine silts and clays. Northeast of the Yukon River, intermediate-resistivity values suggest frozen conditions at depth (Figures 4b and 4c), except under the Porcupine River (Figure 4a), where we interpret unfrozen conditions to dominate.

[13] A number of other potentially unfrozen zones can be seen as vertically extensive low-resistivity regions in the depth images in Figure 3, and are co-located with numerous lakes and ponds, a sinuous side-channel of the Yukon River (indicated by arrows in Figures 3 and 4), and Twelvemile Lake. The black-dashed lines in Figure 4 indicate our interpreted base of permafrost and show that the permafrost layer is absent beneath most of the large surface-water features. In several locations, it is unclear from the resistivity models whether or not there is a through-going unfrozen zone. These locations might represent taliks that have not fully developed or relict taliks that have partially re-frozen. Additional profiles along several of the 'reconnaissance' survey lines (Figure S1 and Text S1 of the auxiliary material) provide a broader view of the hydrogeologic settings within the survey area, and are consistent with features observed in the block portion of the survey as well as the mapped geology (Figure 1).

[14] A three-dimensional view of a large unfrozen zone below a lake is illustrated in Figure 5a, which shows a cutout view of the resistivity model over an area of approximately 24 km^2 surrounding Twelvemile Lake. The gray isosurface embedded in the resistivity image represents our interpretation of the base of permafrost in the subsurface. Unfrozen areas beneath some of the smaller surface-water features are also evident in the subsurface, though it is uncertain if they are fully connected to the sub-permafrost zone. A similar three-dimensional view of about 147 km^2 surrounding the Yukon River is shown in Figure 5b. With the exception of a few small frozen islands, permafrost is absent beneath the river. The base of permafrost deepens rapidly on either side of the river, though it is steepest to the northeast and continues to dip downward gradually to the southwest (Figure 4).

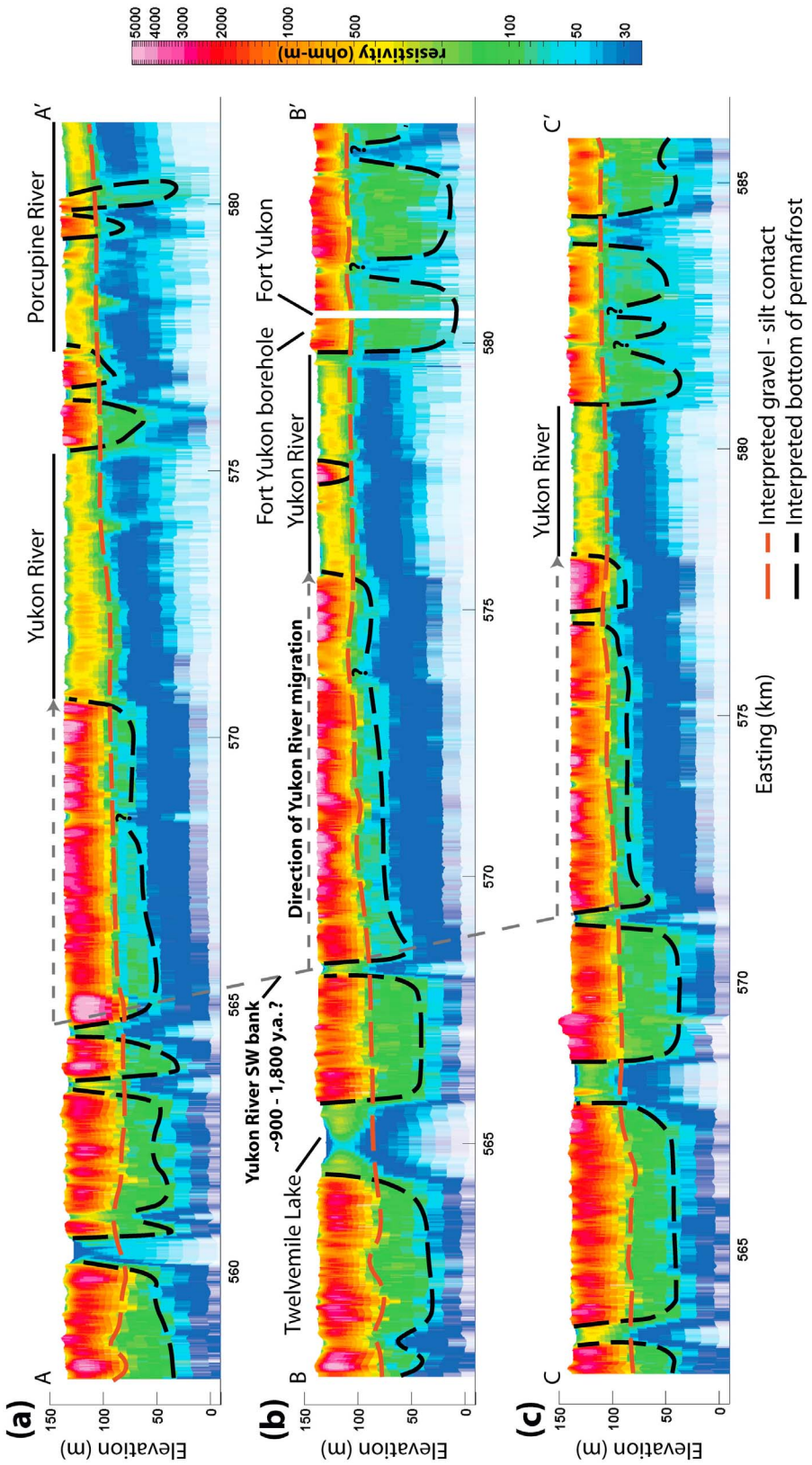

Figure 4. Resistivity cross-sections along the three transects highlighted in Figure 3 with relevant surface features annotated. Arrows indicate the location of a sinuous side-channel of the Yukon River that is also evident as a shallow low-resistivity zone in Figures 3b and 3e. Interpreted lithologic and permafrost boundaries are superimposed as dashed lines. Vertical exaggeration is approximately 25:1.

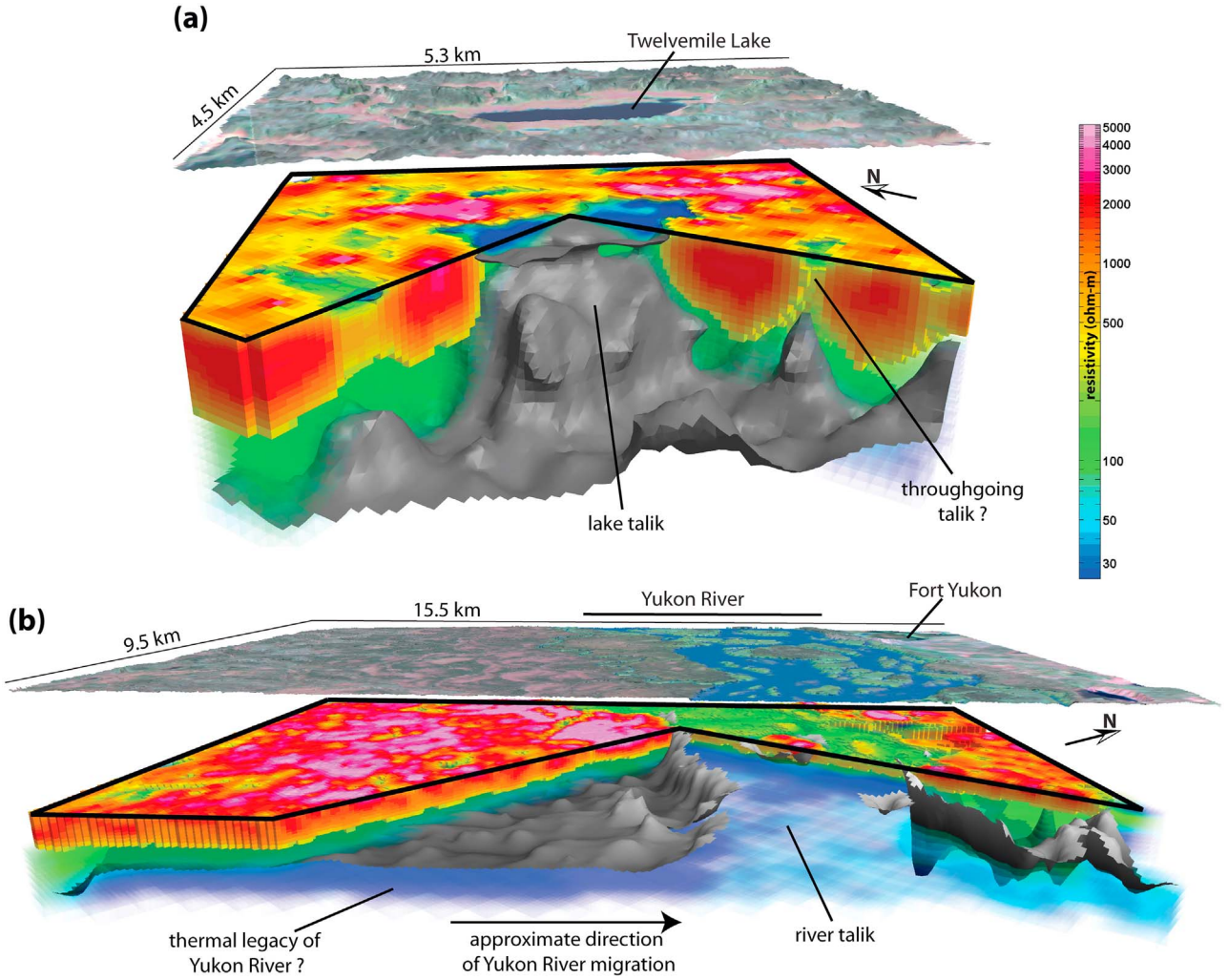

Figure 5. Three-dimensional cutout view of the resistivity model in the vicinity of (a)Twelvemile Lake and (b) the Yukon River. The grey isosurfaces are interpreted to indicate the base of permafrost in the subsurface. The upper image in each figure is a Landsat view of the region displayed below. Vertical exaggeration is 12:1.

4.2. Hydrogeologic and Geomorphologic Implications

[15] Low-resistivity unfrozen zones beneath many of the lakes, ponds, and rivers in the study area likely represent taliks that can form beneath surface-water features [*Grosse et al.*, 2011; *Yoshikawa and Hinzman*, 2003]. Surface water that remains unfrozen in the winter imposes a non-freezing condition on the ground just below, in contrast with adjacent areas of the ground exposed directly to sub-freezing winter temperatures. Therefore, subsurface ice cannot exist permanently below such surface water bodies. Taliks that fully penetrate the entire thickness of permafrost provide pathways for enhanced surface - groundwater interaction and may be associated with shrinking or expanding lakes and ponds [*Roach et al.*, 2011]. Unfrozen zones that do not extend all the way through the permafrost layer appear to correspond with smaller water bodies perched on top of the frozen gravel, or relatively young surface water bodies that have not had sufficient time to develop taliks. Both of these types of features are evident in the AEM survey (Figure 5).

[16] An unexpected finding of the AEM survey is the low-resistivity zone, interpreted as unfrozen, dipping to the southwest from the present-day Yukon River (Figures 4 and 5b). We speculate that this may be a thermal relic of the northward lateral migration of the Yukon River [*Clement*, 1999] that has been recorded in the permafrost. If it was stationary long enough at its historic location to the southwest, the Yukon River would have developed a low-resistivity thaw zone beneath it, as is observed today at its current location. As the river migrated to the north, the ground beneath the old river system would begin to re-freeze from the surface downwards [*Crampton*, 1979]. Using an estimated average lateral migration rate of 5–10 m/yr [*Clement*, 1999], we estimate that the Yukon River system was above the southwestern extent of the low-resistivity zone in Figure 3f approximately 900–1,800 years ago, roughly 9 km to the south and west of its present location (Figure 4). In order for the surface to re-freeze to a depth of ~70 m, these estimates suggest that the permafrost would have to freeze downward at an average rate of approximately 4–8 cm/yr.

[17] Although this hypothesis is only partially constrained, the rates are roughly consistent with observations [*Mackay*, 1997] and numerical simulations [*Ling and Zhang*, 2004]

of taliks that re-freeze after lake drainage. In addition, a very similar permafrost configuration was inferred from borehole observations along a smaller migrating river system in the northern Yukon in Canada [*Crampton*, 1979]. Radiocarbon ages from sand sheets just north of the Yukon River near Fort Yukon suggest that the river has not been north of its present location in the last ~10,000 years [*Froese et al.*, 2005]. This latest Pleistocene age constraint supports our interpretation that the sharp lateral transition in resistivity at the northeast bank of the Yukon River (Figure 4) indicates the boundary where the river is impinging on relatively thick, old permafrost.

[18] Our interpretation is also consistent with the solution to the Stefan problem, where the depth to which permafrost has frozen due to conduction is proportional to the square root of time (i.e. $z \sim c^{*}t^{1/2}$). The constant, c, is related to the thermal properties of the ground, and is typically in the range 1–5 [*Osterkamp and Burn*, 2003]. Given the estimate of 900–1,800 years and the AEM-interpreted base of permafrost ~70 m, we estimate an average value for c during that period to be ~1.6–2.3. Detailed field work in the area, along with more rigorous numerical modeling that also incorporates advective processes [*Ge et al.*, 2011; *Rowland et al.*, 2011], could test this hypothesis more rigorously.

5. Conclusions

[19] Arctic environments have garnered substantial interest because of their relevance to climate, ecosystems, and natural resources. Permafrost is ubiquitous in cold regions, but the details of its distribution, particularly at depth, remain largely unknown. This work highlights a pioneering application of airborne electromagnetic data to provide detailed regional-scale images of permafrost that cannot be achieved with other types of data. Our results offer new insights into the evolution of permafrost systems, evidenced by the thermal legacy of surface and groundwater features, and will be a critical baseline for future permafrost studies. We further expect that these data will have significant implications for studying other coupled hydrologic systems, such as the development and re-freezing of taliks as they undergo variable thermal forcing. Future work will integrate remote sensing data, targeted ground-based geophysics, shallow probing to assess the top of permafrost, geochemical analyses of lake and river samples, and thermally coupled hydrologic modeling to better understand dynamic permafrost-related processes in the Yukon Flats.

[20] **Acknowledgments.** The USGS Climate and Land Use Change Mission Area (Climate Effects Network and R&D Programs) provided funding for the acquisition and interpretation of the AEM data. Additional support for the data processing and interpretation was provided by the USGS Minerals Program through the Geophysical Methods Development project. Fugro Airborne was contracted to acquire the AEM dataset. Darren Van Sistine (USGS) digitized the geologic map that is illustrated in this paper, and Jennifer Rover (USGS) provided the surface water data for the map. We thank Carol Finn, Dan Muhs, Duane Froese, and Richard Reger for their thoughtful reviews of this manuscript.

[21] The Editor thanks Duane Froese and Richard Reger for their assistance in evaluating this paper.

References

Avis, C. A., A. J. Weaver, and K. J. Meissner (2011), Reduction in areal extent of high-latitude wetlands in response to permafrost thaw, *Nat. Geosci.*, *4*(7), 444–448, doi:10.1038/ngeo1160.

Ball, L. B., B. D. Smith, B. J. Minsley, J. D. Abraham, C. I. Voss, M. Deszcz-Pan, and J. C. Cannia (2011), Airborne electromagnetic and magnetic survey data of the Yukon Flats and Ft. Wainwright areas, central Alaska, June 2010, *U.S. Geol. Surv. Open File Rep.*, *2011–1304*, 28 pp.

Bense, V. F., G. Ferguson, and H. Kooi (2009), Evolution of shallow groundwater flow systems in areas of degrading permafrost, *Geophys. Res. Lett.*, *36*, L22401, doi:10.1029/2009GL039225.

Clark, A., C. E. Barker, and E. P. Weeks (2009), Drilling and testing the DOI-04-1A coalbed methane well, Fort Yukon, Alaska, *U.S. Geol. Surv. Open File Rep.*, *2009–1064*, 69 pp.

Clement, D. T. (1999), Fluvial geomorphology of the Yukon River, Yukon Flats, Alaska, MSc thesis, 180 pp., University of Calgary, Calgary, Alberta, Canada.

Crampton, C. B. (1979), Changes in permafrost distribution produced by a migrating river meander in the northern Yukon, Canada, *Arctic*, *32*(2), 148–151.

Duguay, C. R., Z. Tingjun, D. W. Leverington, and V. E. Romanovsky (2005), Satellite remote sensing of permafrost and seasonally frozen ground, in *Remote Sensing in Northern Hydrology: Measuring Environmental Change*, *Geophys. Monogr. Ser.*, vol. 163, edited by R. Duguay and A. Pietroniro, pp. 91–118, AGU, Washington, D. C., doi:10.1029/163GM06.

Ferrians, O. J. (1965), Permafrost map of Alaska, scale 1:2,500,000, *U.S. Geol. Surv. Misc. Geological Invest. Map*, *I-445*, U.S. Geological Survey, Reston, VA.

Froese, D. G., D. G. Smith, and D. T. Clement (2005), Characterizing large river history with shallow geophysics: Middle Yukon River, Yukon Territory and Alaska, *Geomorphology*, *67*(3–4), 391–406, doi:10.1016/j.geomorph.2004.11.011.

Froese, D. G., J. A. Westgate, A. V. Reyes, R. J. Enkin, and S. J. Preece (2008), Ancient permafrost and a future, warmer Arctic, *Science*, *321*(5896), 1648, doi:10.1126/science.1157525.

Ge, S., J. McKenzie, C. Voss, and Q. Wu (2011), Exchange of groundwater and surface-water mediated by permafrost response to seasonal and long term air temperature variation, *Geophys. Res. Lett.*, *38*, L14402, doi:10.1029/2011GL047911.

Grosse, G., V. Romanovsky, T. Jorgenson, K. W. Anthony, J. Brown, and P. P. Overduin (2011), Vulnerability and feedbacks of permafrost to climate change, *Eos Trans. AGU*, *92*(9), 73, doi:10.1029/2011EO090001.

Hoekstra, P., P. V. Sellmann, and A. Delaney (1975), Ground and airborne resistivity surveys of permafrost near Fairbanks, Alaska, *Geophysics*, *40*(4), 641–656, doi:10.1190/1.1440555.

Jorgenson, M. T., C. Racine, J. Walters, and T. Osterkamp (2001), Permafrost degradation and ecological changes associated with a warming climate in central Alaska, *Clim. Change*, *48*(4), 551–579, doi:10.1023/A:1005667424292.

Jorgenson, T., K. Yoshikawa, M. Kanevskiy, Y. Shur, V. Romanovsky, S. Marchenko, G. Grosse, J. Brown, and B. Jones (2008), Permafrost Characteristics of Alaska–A new permafrost map of Alaska, paper presented at Ninth International Conference on Permafrost, Univ. of Alaska Fairbanks, Fairbanks.

Jorgenson, M. T., V. Romanovsky, J. Harden, Y. Shur, J. O'Donnell, E. A. G. Schuur, M. Kanevskiy, and S. Marchenko (2010), Resilience and vulnerability of permafrost to climate change, *Can. J. For. Res.*, *40*, 1219–1236, doi:10.1139/X10-060.

Koven, C. D., B. Ringeval, P. Friedlingstein, P. Ciais, P. Cadule, D. Khvorostyanov, G. Krinner, and C. Tarnocai (2011), Permafrost carbon-climate feedbacks accelerate global warming, *Proc. Natl. Acad. Sci. U. S. A.*, *108*(36), 14,769–14,774, doi:10.1073/pnas.1103910108.

Ling, F., and T. Zhang (2004), Modeling study of talik freeze-up and permafrost response under drained thaw lakes on the Alaskan Arctic Coastal Plain, *J. Geophys. Res.*, *109*, D01111, doi:10.1029/2003JD003886.

Mack, M. C., M. S. Bret-Harte, T. N. Hollingsworth, R. R. Jandt, E. A. G. Schuur, G. R. Shaver, and D. L. Verbyla (2011), Carbon loss from an unprecedented Arctic tundra wildfire, *Nature*, *475*(7357), 489–492, doi:10.1038/nature10283.

Mackay, J. R. (1997), A full-scale field experiment (1978–1995) on the growth of permafrost by means of lake drainage, western Arctic coast: a discussion of the method and some results, *Can. J. Earth Sci.*, *34*(1), 17–33, doi:10.1139/e17-002.

Nelson, F. E., O. A. Anisimov, and N. I. Shiklomanov (2001), Subsidence risk from thawing permafrost, *Nature*, *410*(6831), 889–890, doi:10.1038/35073746.

Nelson, F. E., O. A. Anisimov, and N. I. Shiklomanov (2002), Climate change and hazard zonation in the crcum-Arctic permafrost regions, *Nat. Hazards*, *26*(3), 203–225, doi:10.1023/A:1015612918401.

O'Donnell, J. A., J. W. Harden, A. D. McGuire, M. Z. Kanevskiy, M. T. Jorgenson, and X. Xu (2011), The effect of fire and permafrost interactions on soil carbon accumulation in an upland black spruce ecosystem of interior Alaska: implications for post-thaw carbon loss, *Global Change Biol.*, *17*, 1461–1474, doi:10.1111/j.1365-2486.2010.02358.x.

Osterkamp, T. E. (2007), Characteristics of the recent warming of permafrost in Alaska, *J. Geophys. Res.*, *112*, F02S02, doi:10.1029/2006JF000578.

Osterkamp, T. E., and C. R. Burn (2003), Permafrost, in *Encyclopedia of Atmospheric Sciences*, edited by J. R. Holton, pp. 1717–1729, Academic, Oxford, U. K., doi:10.1016/B0-12-227090-8/00311-0.

Osterkamp, T. E., and V. E. Romanovsky (1999), Evidence for warming and thawing of discontinuous permafrost in Alaska, *Permafrost Periglacial Processes*, *10*(1), 17–37, doi:10.1002/(SICI)1099-1530(199901/03)10:1<17::AID-PPP303>3.0.CO;2-4.

Palacky, G. J. (1987), Resistivity characteristics of geologic targets, in *Electromagnetic Methods in Applied Geophysics*, vol. 1, *Theory*, edited by M. N. Nabighian, pp. 53–129, Soc. of Explor. Geophys., Tulsa, Okla.

Roach, J., B. Griffith, B. Verbyla, and J. Jones (2011), Mechanisms influencing changes in lake area in Alaskan boreal forest, *Global Change Biol.*, *17*, 2567–2583, doi:10.1111/j.1365-2486.2011.02446.x.

Romanovsky, V. E., and T. E. Osterkamp (2000), Effects of unfrozen water on heat and mass transport processes in the active layer and permafrost, *Permafrost Periglacial Processes*, *11*(3), 219–239, doi:10.1002/1099-1530(200007/09)11:3<219::AID-PPP352>3.0.CO;2-7.

Rowland, J. C., B. J. Travis, and C. J. Wilson (2011), The role of advective heat transport in talik development beneath lakes and ponds in discontinuous permafrost, *Geophys. Res. Lett.*, *38*, L17504, doi:10.1029/2011GL048497.

Schuur, E. A. G., J. G. Vogel, K. G. Crummer, H. Lee, J. O. Sickman, and T. E. Osterkamp (2009), The effect of permafrost thaw on old carbon release and net carbon exchange from tundra, *Nature*, *459*(7246), 556–559, doi:10.1038/nature08031.

Siemon, B., A. V. Christiansen, and E. Auken (2009), A review of helicopter-borne electromagnetic methods for groundwater exploration, *Near Surf. Geophys.*, *7*(5–6), 629–646.

Walvoord, M. A., and R. G. Striegl (2007), Increased groundwater to stream discharge from permafrost thawing in the Yukon River basin: Potential impacts on lateral export of carbon and nitrogen, *Geophys. Res. Lett.*, *34*, L12402, doi:10.1029/2007GL030216.

Williams, J. R. (1962), Geologic reconnaissance of the Yukon Flats District Alaska, *U.S. Geol. Surv. Bull.*, *1111-H*, 289–331.

Yoshikawa, K., and L. D. Hinzman (2003), Shrinking thermokarst ponds and groundwater dynamics in discontinuous permafrost near Council, Alaska, *Permafrost Periglacial Processes*, *14*(2), 151–160, doi:10.1002/ppp.451.

Zhang, T., R. G. Barry, K. Knowles, J. A. Heginbottom, and J. Brown (2008), Statistics and characteristics of permafrost and ground-ice distribution in the Northern Hemisphere, *Polar Geogr.*, *31*(1–2), 47–68, doi:10.1080/10889370802175895.

Zimov, S. A., E. A. G. Schuur, and F. S. Chapin (2006), Permafrost and the global carbon budget, *Science*, *312*(5780), 1612–1613, doi:10.1126/science.1128908.

J. D. Abraham, L. B. Ball, M. Deszcz-Pan, B. J. Minsley, and B. D. Smith, Crustal Geophysics and Geochemistry Science Center, U.S. Geological Survey, MS 964, Denver Federal Center, Denver, CO 80225, USA. (bminsley@usgs.gov)

T. A. Ager and L. Anderson, Geology and Environmental Change Science Center, U.S. Geological Survey, Denver Federal Center, Box 25046, MS 980, Denver, CO 80225, USA.

J. C. Cannia, Nebraska Water Science Center, U.S. Geological Survey, 5231 S. 19th St., Lincoln, NE 68512, USA.

M. T. Jorgenson, Alaska Ecoscience, PO Box 80410, Fairbanks, AK 99708, USA.

C. I. Voss, National Research Program, U.S. Geological Survey, 345 Middlefield Rd., Menlo Park, CA 94025, USA.

M. A. Walvoord, National Research Program, U.S. Geological Survey, MS 413, Denver Federal Center, Denver, CO 80225, USA.

T. P. Wellman, Colorado Water Science Center, U.S. Geological Survey, Denver Federal Center, MS 415, Denver, CO 80225, USA.

B. K. Wylie, Earth Resources Observation and Science Center, U.S. Geological Survey, 47914 252nd St., Sioux Falls, SD 57198, USA.